

Double diamond phase in pear-shaped nanoparticle systems with hard sphere solvent

SCHONHOFER, Philipp WA, CLEAVER, Doug <<http://orcid.org/0000-0002-4278-0098>> and SCHRODER-TURK, Gerd E

Available from Sheffield Hallam University Research Archive (SHURA) at:

<https://shura.shu.ac.uk/23137/>

This document is the Accepted Version [AM]

Citation:

SCHONHOFER, Philipp WA, CLEAVER, Doug and SCHRODER-TURK, Gerd E (2018). Double diamond phase in pear-shaped nanoparticle systems with hard sphere solvent. *Journal of Physics D: Applied Physics*, 51 (46), p. 464003. [Article]

Copyright and re-use policy

See <http://shura.shu.ac.uk/information.html>

Double diamond phase in pear-shaped nanoparticle systems with hard sphere solvent

Philipp W. A. Schönhöfer*

*School of Engineering and Information Technology, Mathematics and Statistics,
Murdoch University, 90 South Street, 6150 Murdoch, Western Australia, Australia and
Institut für Theoretische Physik I, Friedrich-Alexander-Universität Erlangen-Nürnberg, Staudtstraße 7, 91058 Erlangen, Germany*

Douglas J. Cleaver

Materials and Engineering Research Institute, Sheffield Hallam University, Sheffield S1 1WB, UK

Gerd E. Schröder-Turk

*School of Engineering and Information Technology, Mathematics and Statistics,
Murdoch University, 90 South Street, 6150 Murdoch, Western Australia, Australia*

(Dated: September 10, 2018)

The mechanisms behind the formation of bicontinuous nanogeometries, in particular *in vivo*, remain intriguing. Of particular interest are the many systems where more than one type or symmetry occurs, such as the Schwarz' Diamond surface and Schoen's Gyroid surface; a current example are the butterfly nanostructures often based on the Gyroid, and the beetle nanostructures often based on the Diamond surface. Here, we present a computational study of self-assembly of the bicontinuous $Pn\bar{3}m$ Diamond phase in an equilibrium ensemble of pear-shaped particles when a small amount of a hard-sphere 'solvent' is added. Our results are based on previous work that showed the emergence of the Gyroid $Ia\bar{3}d$ phase in a pure system of pear-shaped particles [Interface Focus 7, 20160161 (2017)], in which the pear-shaped particles form an interdigitating bilayer reminiscent of a warped smectic structure. We here show that the addition of a small amount of hard spherical particles tends to drive the system towards the bicontinuous $Pn\bar{3}m$ double Diamond phase, based on Schwarz Diamond minimal surface. This result is consistent with the higher degree of spatial heterogeneity of the Diamond minimal surface as compared to the Gyroid minimal surface, with the hard-sphere 'solvent' acting as an agent to relieve packing frustration. However, the mechanism by which this relief is achieved is contrary to the corresponding mechanism in copolymeric systems; the spherical solvent tends to aggregate within the matrix phase, near the minimal surface, rather than within the labyrinthine channels. While it may relate to the specific form of the potential used to approximate the particle shape, this mechanism hints at an alternative way for particle systems to both release packing frustration and satisfy geometrical restrictions in double Diamond configurations. Interestingly, the lattice parameters of the Gyroid and the Diamond phase appear to be commensurate with those of the isometric Bonnet transform.

The ambition and efforts expended to understand and mimic the formation processes of highly complex and functional nanostructures in living organisms mark one of the pillars of modern bio- and soft matter physics research. Particularly the pursuit to compete with the astonishing efficiency and variety of mechanisms which nature developed is a driving force of many recent studies. Prime examples of those structures, which both visualise the functionality but also combine complexity and efficiency, were identified as biological photonic nanomaterials in insects, birds and plants [1–9]. Especially the family of *cubic bicontinuous structures* [10], characterised by two identical and interwoven network-like channel domains (with a dividing interface described by a minimal surface with negative Gauss curvature) has excited more and more curiosity [11]. Besides their impact on optical properties, like structural coloration and circular polarisation effects [6, 12–15] they also bear potential mechanical [16] and transport [17] applications for nanomaterials.

Self-assembly (that is, the spontaneous and collective arrangement of nanoparticles into ordered, long-range microstructures) has proven to be a fundamental evolutionary strategy to generate elaborate patterns which can be described by cubic bicontinuous structures [10, 18–20]. The $Ia\bar{3}d$

double Gyroid, famously adopted by amphiphilic molecules, for instance in the inverse lipid/water phase without excess water [21–23] – occurs for example during the development process of the single Gyroid structure within wing scales of certain butterflies [24–31]. Here, in an intermediate stage of wing development, it is conjectured that the molecules form bilayers with the same morphology as the Gyroid minimal surface, which act as a membrane separating space into two percolating channels. It has been argued that this bilayer arrangement functions as a cast to externally extruded chitinous cuticle resulting in the final chiral single Gyroid structure, where only one domain is filled with chitin [25, 32] and which causes a bright green appearance of the butterfly [31] (see FIG. 1). Even though experiments showed that similarly other lyotropic and thermotropic liquid crystals [33–35], diblock copolymers [36–41] and dendrimers [42] form various cubic bicontinuous phases, the exact construction mechanisms of many biological systems are not fully understood. Likewise distinct differences between the biological and chemical system remain, in particular with respect to the attainable length scales [43–45], the single/double symmetry and chiral imbalance [27, 30, 46, 47].

Another unsolved phenomenon is the structural trans-

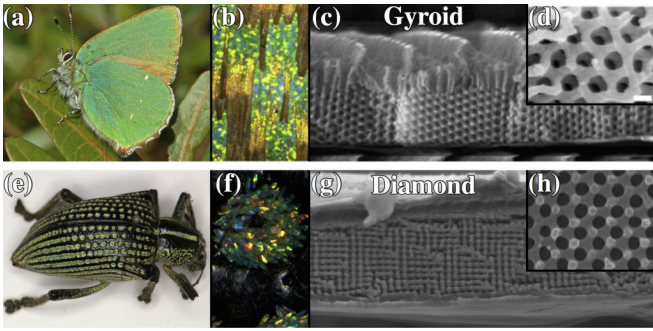


FIG. 1: The nanostructures creating structural color in the *Callophrys rubi* butterfly (a-d) and the *Entimus imperialis* weevil (e-h) are shown. Light microscopy shows that the wings (b) and pits (f) are built out off multi-faceted scales. Electron microscopy of the section of those scales reveals the single Gyroid in the [110]-direction (c,d) with lattice constant $a_{SG}=311$ nm [26] and the single Diamond in the [100]- (g) and [111]-direction (h) with lattice constant $a_{SD}=445$ nm [6]. We were permitted to reproduce the figures from Ref. [28] (a-d) and Ref. [6] (e-h).

formation at the phase transition between different cubic bicontinuous structures which are observed in various lipid [48, 49] and copolymer systems [50–53]. The most common and most studied transition, both experimentally [49, 54, 55] and theoretically [19, 56], is between the double Gyroid and the $Pn\bar{3}m$ double Diamond phase. Similar to the Gyroid, also the Diamond structure (more precisely the single Diamond, where only one channel of the double Diamond network is filled with material) entails interesting optical effects and is spread among insects like butterflies or weevils (see FIG. 1) to create color [6, 7, 57, 58]. Whilst both double symmetric structures can be transformed by Bonnet transformations mathematically [21], the Bonnet pathway causes self-intersections and has to be classified as unphysical [54]. However, a tetragonal transition model was introduced by Fodgen and Hyde, which fulfills the Bonnet relation and maintains both topology and mean-zero curvature along the transition [19, 56]. Based on this Squires *et al.* [49] and later Oka [55] could develop a pictorial representation of the mechanism. The second proposed rhombohedral pathway, which involves the P-surface structure as an intermediate state, was considered energetically less favourable in regards to curvature and packing homogeneity [19]. Here, we also point towards recent work by Chen and Weber on further mathematical transition models [59].

In previous computational studies we obtained a $Ia\bar{3}d$ double Gyroid phase in a self-assembly process of simple pear-shaped particles, that is, convex rotationally-symmetric elongated particles with one wide and one narrow end [60, 61]. At the time, while simulating the phase using the hard limit of a soft potential, we considered the process to be essentially a hard-core potential. However, the potential exhibits deviations from the exact hard-body interactions. As depicted in FIG. 2 those variations can lead to small overlaps

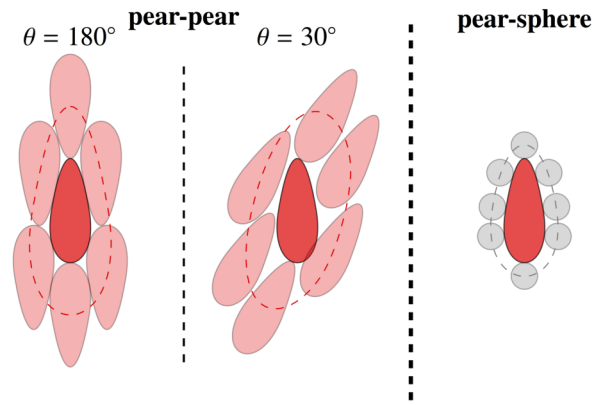


FIG. 2: The interactions between two pear-shaped particles (left) and between a pear-shaped particle and a sphere (right) using modified parametric hard Gauss overlap approximation (PHGO) are sketched. The pear-sphere interaction coincides with the hard body interaction exactly and causes no overlap. Similarly two antiparallel pear particles ($\theta = 180^\circ$) do not display any variations to the exact hard pear-pear interactions (left). However, for other angles between two pears the pear-pear overlap function can underestimate or overestimate the minimal distance which can lead to small overlaps of the blunt ends or gaps between the particles. The greatest overlap occurs for $\theta = 30^\circ$ (middle). The dashed lines indicate the contact profiles around the pear for a given second particle.

or gaps depending of the angle between the pear-shaped particles. For detailed information about its influence on the phase we refer to Ref. [62]. Next to the orientationally ordered nematic and smectic phases the pear-shaped particles form a phase of curved interdigitating bilayers which was identified as the double Gyroid structure (see FIG. 3). The particles arrange in interdigitated bilayers (blunt/wide ends towards the network domains and thin ends near the minimal surface) and revealed a way of particles to satisfy geometrical constraints accompanied by negatively curved bilayers collectively rather than individually.

In the following, we extend this model to show that small quantities of a solvent in the pear system stabilises the $Pn\bar{3}m$ double Diamond phase (in addition to the double Gyroid phase). By ‘solvent’ we here mean spherical particles that interact via hard-core interactions with the pear-shaped particles and with each other. The inclusion of a solvent is motivated by the fact that the double Diamond has greater spatial heterogeneities [18] and that a solvent can release frustration related to them. The stabilization of the double Diamond structure was indeed also observed in diblock copolymers upon addition of extra homopolymer [39]. Here, the additional particles accumulate at the backbone of the labyrinth-like domains, which can not be homogenously occupied by the diblock copolymers without causing unfavourable gaps. The added solvent also leads to the formation of the double Diamond in the pear particle system, however, as we show in the following the heterogeneities are differently resolved by plac-

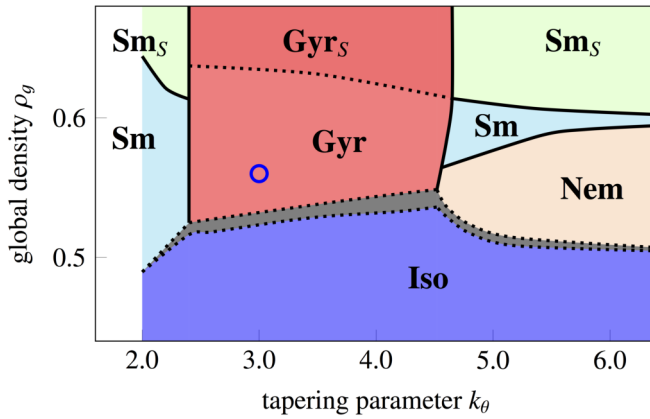


FIG. 3: A sketch of the phase diagram of a monodisperse system of purely repulsive (but not strictly hard-core) pear-shaped particles obtained from Ref. [61]. The blue circle indicates roughly the parameters of the Gyroid system from which we here obtain the Diamond structure by adding a ‘hard sphere solvent’.

ing the supplementary material in the dividing matrix rather than in the channel domains.

MOLECULAR DYNAMICS OF MIXTURES OF SPHERE AND PEAR-SHAPED PARTICLES

We perform Molecular Dynamics (MD) simulations of pear-shaped particles with a small concentration of hard spheres which plays role of a solvent. For the interactions between the hard-core particles we use a parametric hard Gaussian overlap (PHGO) approximation [63], which can be modified to describe interactions believed to be [64] similar to those between purely repulsive pear-shaped particles and to the hard-core interaction between a spherical and pear-shaped particle. This approach contains an approximation to calculate the contact distance between a pear with another particle by the overlap function of a locally equivalent encasing ellipsoid (details are given in [63, 64]). Here we have to mention, however, that even though this overlap function results in a precise hard body interaction between pears and spheres, the pear-pear interaction reveals some inaccuracies. This can cause the blunt ends of pears to slightly overlap (around 1.2 % in volume) and reach areas which can not be obtained by hard spheres (see FIG. 2). The simulations are carried out using the same methodology as in [61], adjusted to include the hard-sphere solvent. The system is set up within a cubic box with three-dimensional periodic boundary conditions, with an overall particle packing fraction $\rho = 0.56$ and a 1:9 volume ratio of solvent particles to pear-shaped particles ($v = \frac{V_p}{V_{sp}} = 9$). The aspect ratio of the pear-shaped particles k is set to 2.75 and the so called tapering parameter k_θ tapering angle is set to 3 (this corresponds to a tapering angle of 19°). The particle shape is shown, to scale, in FIG. 2. The mixture is in the dry limit with a low number of spheres $N_{sp}=90$ and a majority

of pears $N_p=820$ ($n = \frac{N_p}{N_{sp}} = \frac{82}{9}$). Additionally, the MD simulations are performed in the canonical (NVT) ensemble, with a time step $\Delta t=0.0015$ and dimensionless temperature $T=1$ (the Boltzman constant is set to $k_B=1$), since phase behaviour at fixed density is independent of the temperature for hard-core particle systems and can be seen as a scaling parameter [65]. All simulations are run for 20.000.000 time steps. The systems seem to reach sufficient equilibration to identify the Diamond phase after around 5.000.000 steps.

SELF-ASSEMBLY OF BICONTINUOUS PHASES IN PEAR SPHERE SYSTEMS

By starting the simulations from a low density ($\rho=0.3$) and slowly compressing the system to a packing fraction where the double Gyroid forms in a monodisperse pear-particle system ($\rho>0.54$), we can ensure that the developed macrostructure is not enforced by the initial conditions but assembles from an unordered isotropic phase. The obtained morphology of all 20 simulation runs, generated from different isotropic initial conditions, corresponds to a $2 \times 2 \times 2$ unit cell of the bicontinuous double Diamond network structure (see FIG. 4). Additionally, we also generated an artificial smectic phase as an initial starting configuration which proves to be unstable and eventually turns into the double Diamond phase as well. The resemblance to the double Diamond structure becomes apparent by extracting both labyrinth domains and depicting only the position of the blunt ends by spheres. The resulting set of points can be separated nicely by the double Diamond minimal surface. Additionally, the set reveals the typical 2- and 3-fold rotation symmetry along the [100]- and [111]-direction. Their 2D projections lead to square ([100]-direction) and hexagonal ([111]-direction) patterns which match perfectly with the graph of the cubic Diamond structure (as well as the 2D projections in the [110]-direction; see FIG. 4).

In our simulations we observe the same spatial arrangement of pear-shaped particles as described previously for the double Gyroid: The particles interdigitate with their thin ends at the minimal surface interface and form the two double Diamond network domains with their blunt (wider) ends as sketched in FIG. 4. The interdigitation, where pears effectively protrude through the minimal surface, collectively leads to an effectively wider space per molecule near the minimal surface. Like in the Gyroid phase this finding is fundamentally different to the intuitive interpretation of the molecular shape concept [66, 67], which holds for lipid or di-block copolymer systems mentioned above, where for negatively curved surfaces the space occupied by an individual particle maximises at the membrane and decreases in normal direction.

To investigate, however, why the double Diamond is favoured over the Gyroid, we have to look at the position of

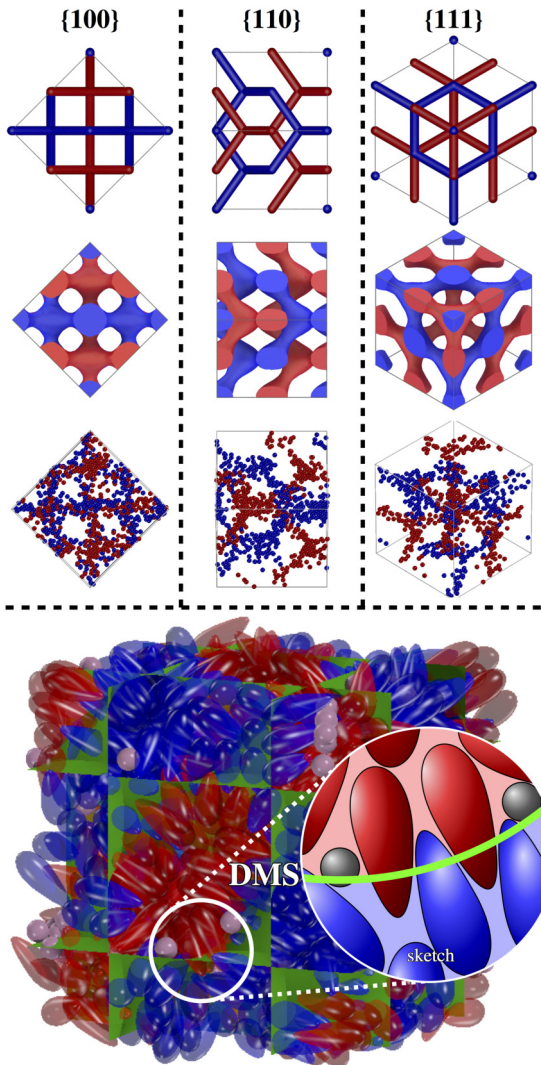


FIG. 4: An assembly of 820 pear-shaped particles and 90 hard-core spheres forming the $2 \times 2 \times 2$ unit cell of the double Diamond structure ($k = 2.75$, $\alpha = 19^\circ$, $\rho = 0.56$, $v = 9, n = \frac{82}{9}$). Positions of the blunt ends determine to which of the two distinct domains (red/blue) the particle belongs. The green surface represents the double Diamond minimal surface (DMS) which separates these domains. The spherical segment is a 2 dimensional sketch, recreated from the indicated part in the pear-particle system to highlight the special arrangement of particles. On the top only the position of the blunt ends are depicted as spheres to showcase the labyrinth-like channels (3rd row). The system is shown in the [100]-, [110]- and [111]-direction and compared with the skeletal-graph (first row) and the channel domain (2nd row) of the double diamond structure. The latter is generated using the nodal approximation of the double diamond.

the spherical solvent. Like the arrangement of the pear-shaped particles also the dominant location of the solvent particles in the simulations interestingly differs from the intuitive guess and earlier findings in other double Diamond forming systems. For example, studies on diblock copolymers show that the packing frustration is released by the solvent/additional material – in this case homopolymers – swelling the network

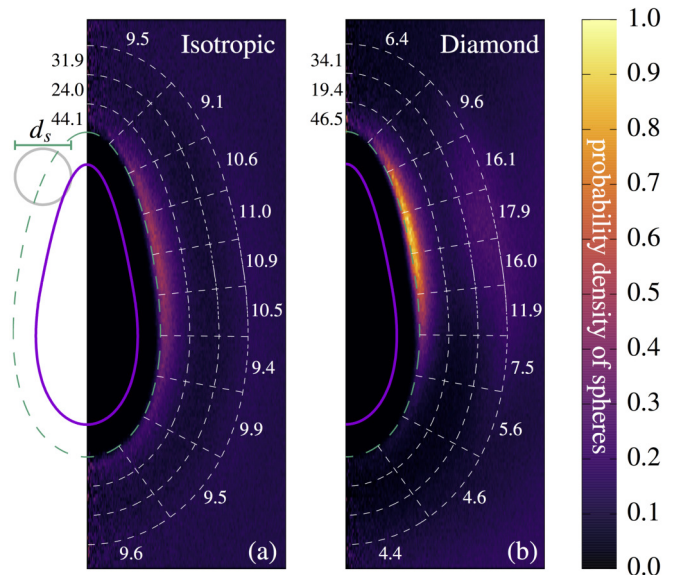


FIG. 5: The 2 dimensional pear-sphere-correlation function $g(z, r)$ of a system in the isotropic phase (a) and the cubic Diamond phase (b) is shown. z is the distance between the pears and spheres central position along the orientation vector of the pear-shaped particle. r is the radial component of the distance between the pear and sphere center. The dashed white lines determine the parallel surface of the pear particles. The small numbers indicate the distribution of sphere particles within a given radial (black) or polar (white) sector in percentage. Only particles lying within the outmost drawn parallel surface are considered.

domain [39]. In our simulation this would correspond to the hard spheres aggregating at the blunt ends of the pear-particles and fill space within the channel domains. The 2-dimensional pear-sphere pair correlation function, however, reveals a largely opposite behaviour (see FIG. 5). In the isotropic phase the spheres distribute uniformly around the pear particles without any greater preference. By increasing the density, however, the spheres are ‘pushed’ towards the thin ends of the pears where, as seen in FIG. 5b, a higher concentration of spheres can be observed. This coincides with the aggregation of spheres around the minimal surface (FIG. 6a shows a symmetric bell-shaped distribution), such that the solvent fills additional space where the pears interdigitate. Note here that this mechanism benefits from the earlier addressed small disparities between the perfect hard body interactions and the used PHGO potential. Consequently, we have to take the role of minor non-additivity effects between pear-shaped particles into account which probably enhance the overall tendency of spheres to gather around the thin rather than the blunt ends of pears.

To determine the location of the spheres in more detail we identify the Gauss curvature of each point on the Diamond minimal surface which is closest to the center of a hard sphere. FIG. 6b indicates that the majority of spheres are located around areas with high negative Gauss curvature.

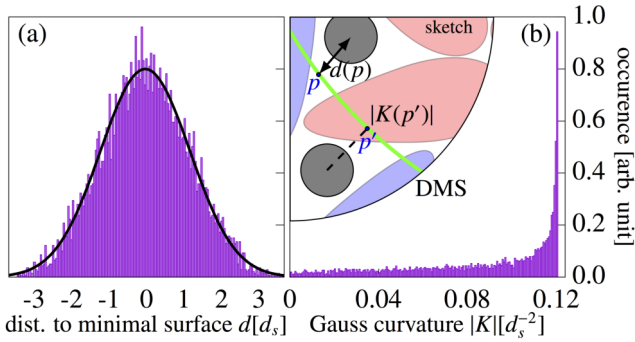


FIG. 6: (a) The distribution of spheres around the Diamond minimal surface is displayed. Therefore, the distance $d(x) := \inf\{\text{dist}(x, q) | q \in \text{DMS}\}$ of each solvent particle to its closest point $p \in \text{DMS}$ where $\text{dist}(x, p) = d(x)$ on the Diamond minimal surface (DMS – indicated in green) is calculated. Positive/Negative distances imply that the sphere lies in the red/blue channel domain. The black line indicates a Gaussian fit to highlight the bell-shaped distribution. (b) The position distribution of the spheres in regards to Gauss curvature is plotted. Here, the absolute value of the Gauss curvature $|K(p)|$ at its closest point p on the DMS is assigned to each solvent particle $|K(x)| := |K(p)|$.

This observation is consistent with the local effect of spheres on their surrounding pear particles. By aggregating close to the thin ends of the pears the spheres act as ‘disruptive’ elements between the interdigitating pear sheets and hinder pears to protrude into the opposite domain (see sketch in FIG. 4). However, they also force neighbouring pears to arrange in a much wider angle and, therefore, induce a greater amount of negative curvature in the system. This mechanism bears resemblance to lipid bilayers where proteins can be inserted within the membrane like ‘wedges’ and act as either curvature relief or a curvature generation agents [68, 69].

The implementation of spheres to create curvature might be also an explanation for the stabilisation and preference of the double Diamond phase over the double Gyroid in general. In our earlier studies [61] we determined a correlation between the interdigitation depth and the local Gauss curvature of the system. The further pears reach into the realm of the opposite channel system, the more curvature is contributed to the interface between both pear particle clusters. In case of the Gyroid and Diamond minimal surface formed by the pear-particle systems the maximum negative Gauss curvature is roughly the same. By comparing the unit cell length between the Diamond a_D (half of the simulation box size) and the Gyroid phase of the monodisperse pear-shaped particle system a_G , which was determined by scattering functions (see FIG. 9 in Ref. [61]), we can identify the unit cell size ratio $\frac{a_G}{a_D} = 1.54$. Thus, within the uncertainties and experimental parameters, it seems that both bicontinuous phases are related by the Bonnet transformation, which causes a ratio $\frac{a_G}{a_D} = 1.576$ [18, 21, 70], and hence isometric. Isometric minimal surfaces are locally indistinguishable and, therefore, preserve area and Gauss curvature [18]. This, however, causes two issues in forming

the Diamond structure, which can not be resolved solely by pear particles simultaneously. In the Diamond phase pears are not able to interdigitate as deeply as in the Gyroid phase without creating gaps in the channel domain. Similarly by filling the gaps with their blunt ends, the pear bilayers are less interdigitated such that they lose their capability to generate enough curvature via interdigitation. Consequently, there are technically two possible mechanisms how additional material can stabilise the double Diamond. Firstly the spheres can fill the gaps in the channel domains, such that the pears can penetrate the minimal surface efficiently. In the second and apparently more favourable mechanism the pears occupy the space around the labyrinth backbone and the system compensates its loss in creating high negative Gauss curvature by interdigitation by placing the solvent at the minimal surface and by increasing locally the amount of curvature accordingly.

Note that we here only assert the formation of the double Diamond for a simulation box of size $(2a)^3$ where a is the lattice parameter of the $\text{Pn}\bar{3}\text{m}$ unit cell. For a system which theoretically should form $4 \times 4 \times 4$ unit cells ($N_p=6560$, $N_{sp}=720$) we have not achieved a clear identification of the symmetry of the double Diamond. Even though we still observe interdigitation the system forms singular nodes characteristic for both the double diamond (4 branched nodes) and the double gyroid (3 branched nodes). This leads to the assumption that the particle number/size ratio to form a pure double diamond phase might not be chosen perfectly. Smaller systems (like the $2 \times 2 \times 2$ system) can distribute the extra material more easily and consequently, better conform to a potential lack of additional material, whereas for larger systems an insufficient distribution of the solvent spheres can locally cause areas with low concentration of spheres expressed in the formation of a gyroid-like, and some areas with a larger concentration of spheres sufficient to enable stabilisation of a diamond-like channel system.

To summarize, we have shown using computational simulation that the introduction of small quantities of hard spheres appears to stabilize the bicontinuous $\text{Pn}\bar{3}\text{m}$ cubic Diamond phase in pear-shaped particle system. In the process the system showcases a new way to overcome the additional spatial heterogeneities in relation to the double Gyroid phase by placing the spheres around the minimal surface and aiding the system to create surfaces of high negative Gauss curvature. This observation gives rise to an alternative perspective on self-assembly processes and can lead to helpful insight and a further step to answer the unknown questions in structure formation in nature. In terms of new synthesis strategies our results can give an outlook to new possible methods to form the double diamond out of the gyroid morphology. For example some molecules forming cubosomes can swell certain domains of the cubosome by addition of a low concentration of a solvent/other material [44, 71]. Designing molecules with solvophilic ends which are placed within the separating matrix domain rather than

within the channel domain should bear the capability to form double diamond nanostructures in a similar fashion like the pear-shaped particle system. Additionally, we could yield information that the Diamond phase is related to the Gyroid phase by a Bonnet transformation. Whether or not one would expect the Diamond structure in the beetles and the Gyroid structure in the butterflies to be Bonnet relatives of one another is a subtle question, and well beyond this article. We will here not delve into that question, and cannot even offer a firm assessment if the lattice parameters correspond to those of Bonnet-related Gyroid and Diamond structures (The values are $a_{SG}=311$ nm [26] for the single Gyroid and $a_{SD}=445$ nm [6] for the single Diamond). However, linked by the Bonnet relation the pear-shaped particle system bears the opportunity for future studies to investigate the possible transitions between both phases [19, 56, 59]. Note that the parameter space for the pear-sphere system is vast (including k , k_θ , ρ , n , v) and our results presented here are not a systematic study of this parameter space. A comprehensive investigation should follow, however, probably best undertaken when the question of non-additivity and differences to a true pear-pear hardcore potential are fully understood [62].

We thank Universities Australia and the German Academic Exchange Service (DAAD) for funds through a collaboration funding scheme, through the grant “Absorption and confinement of complex fluids”. We also thank the DFG through the ME1361/11-2 and SCHR1148/3-2 grants for funding. We gratefully acknowledge Matthieu Marechal for multiple fruitful discussions about the pear-shaped particle system and Bodo Wilts for making some of the images of FIG. 1 available and a careful reading of the manuscript. P.W.A.S. acknowledges a Murdoch University Postgraduate Research Scholarship and travel funding for this research by the Australian Institute of Physics.

* P.Schoenhoefner@murdoch.edu.au

- [1] M. Srinivasarao, Chem. Rev. **99**, 1935 (1999).
- [2] P. Vukusic and J. R. Sambles, Nature **424**, 852 (2003).
- [3] J. Zi, X. Yu, Y. Li, X. Hu, C. Xu, X. Wang, X. Liu, and R. Fu, Proc. Natl. Acad. Sci. USA **100**, 12576 (2003).
- [4] V. Sharma, M. Crne, J. O. Park, and M. Srinivasarao, Science **325**, 449 (2009).
- [5] S. Vignolini, P. J. Rudall, A. V. Rowland, A. Reed, E. Moyroud, R. B. Faden, J. J. Baumberg, B. J. Glover, and U. Steiner, Proc. Natl. Acad. Sci. USA **109**, 15712 (2012).
- [6] B. D. Wilts, K. Michielsen, J. Kuipers, H. De Raedt, and D. G. Stavenga, Proc. R. Soc. London. Ser. B, rspb20112651 (2012).
- [7] B. D. Wilts, K. Michielsen, H. De Raedt, and D. G. Stavenga, J. R. Soc. Interface **9**, 1609 (2012).
- [8] V. Sharma, M. Crne, J. O. Park, and M. Srinivasarao, Mater. Today **1**, 161 (2014).
- [9] B. D. Wilts, K. Michielsen, H. De Raedt, and D. G. Stavenga, Proc. Natl. Acad. Sci. USA **111**, 4363 (2014).
- [10] A. H. Schoen, NASA Technical Note, TD (1970).
- [11] L. Han and S. Che, Adv. Mater. **30**, 1705708 (2018).
- [12] Y. Deng and M. Mieczkowski, Protoplasma **203**, 16 (1998).
- [13] Z. A. Almsharqi, S. D. Kohlwein, and Y. Deng, J. Cell Biol. **173**, 839 (2006).
- [14] B. G. Tenchov, R. C. MacDonald, and D. P. Siegel, Biophys. J. **91**, 2508 (2006).
- [15] J. A. Dolan, B. D. Wilts, S. Vignolini, J. J. Baumberg, U. Steiner, and T. D. Wilkinson, Adv. Opt. Mater. **3**, 12 (2015).
- [16] S. C. Kapfer, S. T. Hyde, K. Mecke, C. H. Arns, and G. E. Schröder-Turk, Biomaterials **32**, 6875 (2011).
- [17] L. Sagalowicz and M. E. Leser, Curr. Opin. Colloid Interface Sci. **15**, 61 (2010).
- [18] G. E. Schröder, S. J. Ramsden, A. G. Christy, and S. T. Hyde, Eur. Phys. J. B **35**, 551 (2003).
- [19] G. E. Schröder-Turk, A. Fogden, and S. T. Hyde, Eur. Phys. J. B **54**, 509 (2006).
- [20] I. Prasad, H. Jinnai, R.-M. Ho, E. L. Thomas, and G. M. Gration, Soft Matter **14**, 3612 (2018).
- [21] S. Hyde and S. Andersson, Z. Kristallogr. - Cryst. Mater. **168**, 213 (1984).
- [22] K. Larsson, J. Phys. Chem. **93**, 7304 (1989).
- [23] J. M. Seddon and R. H. Templer, Phil. Trans. R. Soc. Lond. A **344**, 377 (1993).
- [24] K. Michielsen and D. G. Stavenga, J. Roy. Soc. Interface **5**, 85 (2008).
- [25] V. Saranathan, C. O. Osuji, S. G. Mochrie, H. Noh, S. Narayanan, A. Sandy, E. R. Dufresne, and R. O. Prum, Proc. Natl. Acad. Sci. USA **107**, 11676 (2010).
- [26] G. E. Schröder-Turk, S. Wickham, H. Averdunk, F. Brink, J. F. Gerald, L. Poladian, M. Large, and S. Hyde, J. Struct. Biol. **174**, 290 (2011).
- [27] C. Mille, E. C. Tyrode, and R. W. Corkery, RSC Adv. **3**, 3109 (2013).
- [28] M. Saba, B. D. Wilts, J. Hielscher, and G. E. Schröder-Turk, Mater. Today **1**, 193 (2014).
- [29] S. Yoshioka, H. Fujita, S. Kinoshita, and B. Matsuhana, J. Roy. Society Interface **11**, 20131029 (2014).
- [30] B. Winter, B. Butz, C. Dieker, G. E. Schröder-Turk, K. Mecke, and E. Spiecker, Proceedings of the National Academy of Sciences **112**, 12911 (2015).
- [31] B. D. Wilts, B. A. Zubiri, M. A. Klatt, B. Butz, M. G. Fischer, S. T. Kelly, E. Spiecker, U. Steiner, and G. E. Schröder-Turk, Science advances **3**, e1603119 (2017).
- [32] H. Ghiradella, in *Advances in Insect Physiology*, Vol. 38 (Elsevier, 2010) pp. 135–180.
- [33] P. Barois, S. Hyde, B. Ninham, and T. Dowling, Langmuir **6**, 1136 (1990).
- [34] T. Ichikawa, M. Yoshio, A. Hamasaki, J. Kagimoto, H. Ohno, and T. Kato, J. Am. Chem. Soc. **133**, 2163 (2011).
- [35] H. M. G. Barriga, M. N. Holme, and M. M. Stevens, Angew. Chem. (2018).
- [36] M. W. Matsen and M. Schick, Phys. Rev. Lett. **72**, 2660 (1994).
- [37] D. A. Hajduk, P. E. Harper, S. M. Gruner, C. C. Honeker, G. Kim, E. L. Thomas, and L. J. Fetters, Macromolecules **27**, 4063 (1994).
- [38] G. Schröder-Turk, A. Fogden, and S. Hyde, Euro. Phys. J. B **59**, 115 (2007).
- [39] F. J. Martinez-Veracoechea and F. A. Escobedo, Macromolecules **42**, 1775 (2009).
- [40] M. Müller and D.-W. Sun, Phys. Rev. Lett. **111**, 267801 (2013).
- [41] D.-W. Sun and M. Müller, Phys. Rev. Lett. **118**, 067801 (2017).
- [42] X. Zeng, G. Ungar, and M. Impéror-Clerc, Nat. Mat. **4**, 562 (2005).
- [43] H. Barriga, A. Tyler, N. McCarthy, E. Parsons, O. Ces, R. Law,

- J. Seddon, and N. Brooks, *Soft Matter* **11**, 600 (2015).
- [44] H. Kim, Z. Song, and C. Leal, *Proc. Natl. Acad. Sci. USA* **114**, 10834 (2017).
- [45] A. Zabara, J. T. Y. Chong, I. Martiel, L. Stark, B. A. Cromer, C. Speziale, C. J. Drummond, and R. Mezzenga, *Nat. Commun.* **9**, 544 (2018).
- [46] W. Zhao, T. P. Russell, and G. M. Grason, *Phys. Rev. Lett.* **110**, 058301 (2013).
- [47] G. M. Grason, *ACS Macro Lett.* **4**, 526 (2015).
- [48] J. Seddon and R. Templer, *Structure and dynamics of membranes* (Elsevier, Amsterdam, 1995) pp. 97–160.
- [49] A. M. Seddon, J. Hallett, C. Beddoes, T. S. Plivelic, and A. M. Squires, *Langmuir* **30**, 5705 (2014).
- [50] C.-Y. Chu, W.-F. Lin, J.-C. Tsai, C.-S. Lai, S.-C. Lo, H.-L. Chen, and T. Hashimoto, *Macromolecules* **45**, 2471 (2012).
- [51] H. Takagi, K. Yamamoto, and S. Okamoto, *Europhysics Lett.* **110**, 48003 (2015).
- [52] X. Cao, D. Xu, Y. Yao, L. Han, O. Terasaki, and S. Che, *Chem. Mat.* **28**, 3691 (2016).
- [53] W. Mao, X. Cao, Q. Sheng, L. Han, and S. Che, *Angew. Chem.* **129**, 10810 (2017).
- [54] A. M. Squires, R. Templer, J. Seddon, J. Woenkhaus, R. Winter, T. Narayanan, and S. Finet, *Phys. Rev. E* **72**, 011502 (2005).
- [55] T. Oka, *Langmuir* **31**, 11353 (2015).
- [56] A. Fogden and S. T. Hyde, *Eur. Phys. J. B* **7**, 91 (1999).
- [57] J. W. Galusha, L. R. Richey, J. S. Gardner, J. N. Cha, and M. H. Bartl, *Phys. Rev. E* **77**, 050904 (2008).
- [58] J. W. Galusha, M. R. Jorgensen, and M. H. Bartl, *Adv. Mater.* **22**, 107 (2010).
- [59] H. Chen and M. Weber, arXiv preprint arXiv:1804.01442 (2018).
- [60] L. J. Ellison, D. J. Michel, F. Barmes, and D. J. Cleaver, *Phys. Rev. Lett.* **97**, 237801 (2006).
- [61] P. W. A. Schönhöfer, L. J. Ellison, M. Marechal, D. J. Cleaver, and G. E. Schröder-Turk, *Interface Focus* **7**, 20160161 (2017).
- [62] P. W. A. Schönhöfer, M. Marechal, D. J. Cleaver, and G. E. Schröder-Turk, in preparation (2018).
- [63] R. Berardi, M. Ricci, and C. Zannoni, *ChemPhysChem* **2**, 443 (2001).
- [64] F. Barmes, M. Ricci, C. Zannoni, and D. J. Cleaver, *Phys. Rev. E* **68**, 021708 (2003).
- [65] D. Frenkel and B. Smit, *Understanding Molecular Simulation: From Algorithms to Applications* (Computational Science Series, Academic Press, Orlando, 2002).
- [66] J. N. Israelachvili, D. J. Mitchell, and B. W. Ninham, *J. Chem. Soc., Faraday Trans. 2* **72**, 1525 (1976).
- [67] S. Hyde, Z. Blum, T. Landh, S. Lidin, B. Ninham, S. Andersson, and K. Larsson, *The language of shape: the role of curvature in condensed matter: physics, chemistry and biology* (Elsevier, 1996).
- [68] H. T. McMahon and J. L. Gallop, *Nature* **438**, 590 (2005).
- [69] J. Zimmerberg and M. M. Kozlov, *Nat. Rev. Mol. Cell Bio.* **7**, 9 (2006).
- [70] J. M. Seddon, A. M. Squires, C. E. Conn, O. Ces, A. J. Heron, X. Mulet, G. C. Shearman, and R. H. Templer, *Philos. Trans. Royal Soc. A* **364**, 2635 (2006).
- [71] D. Demurtas, P. Guichard, I. Martiel, R. Mezzenga, C. Hébert, and L. Sagalowicz, *Nat. Commun.* **6**, 8915 (2015).